

Optical Transition Energies for Carbon Nanotubes from Resonant Raman Spectroscopy: Environment and Temperature Effects

C. Fantini,¹ A. Jorio,¹ M. Souza,¹ M. S. Strano,² M. S. Dresselhaus,³ and M. A. Pimenta¹

¹*Departamento de Física, Universidade Federal de Minas Gerais, Belo Horizonte, MG, 30123-970 Brazil*

²*Department of Chemical and Biomolecular Engineering, University of Illinois at Urbana/Champaign, Urbana, Illinois 61801, USA*

³*Department of Physics and Department of Electrical Engineering and Computer Science, Massachusetts Institute of Technology, Cambridge, Massachusetts 02139-4307, USA*

(Received 23 April 2004; published 29 September 2004)

This Letter reports the laser energy dependence of the Stokes and anti-Stokes Raman spectra of carbon nanotubes dispersed in aqueous solution and within solid bundles, in the energy range 1.52–2.71 eV. The electronic transition energies (E_{ii}) and the radial breathing mode frequencies (ω_{RBM}) are obtained for 46 different (18 metallic and 28 semiconducting) nanotubes, and the (n, m) assignment is discussed based on the observation of geometrical patterns for E_{ii} versus ω_{RBM} graphs. Only the low energy component of the E_{11}^M value is observed from each metallic nanotube. For a given nanotube, the resonant window is broadened and down-shifted for single wall carbon nanotube (SWNT) bundles compared to SWNTs in solution, while by increasing the temperature, the E_{22}^S energies are redshifted for $S1 [(2n + m) \bmod 3 = 1]$ nanotubes and blueshifted for $S2 [(2n + m) \bmod 3 = 2]$ nanotubes.

DOI: 10.1103/PhysRevLett.93.147406

PACS numbers: 78.30.Na, 63.22.+m, 78.20.Bh, 78.66.Tr

Single wall carbon nanotubes (SWNTs) have been the focus of intensive work for fundamental studies, and are a potential nanomaterial for applications involving interdisciplinary fields, joining physics, chemistry, and biology [1]. Different kinds of SWNTs, as determined by their tubular structures, i.e., diameter (d_i) and chiral angle (θ), exhibit different properties [1]. The characterization of nanotube structures, given by their indices (n, m) is, therefore, of major importance for the development of carbon nanotube science and applications.

Resonance Raman spectroscopy (RRS) [2], optical absorption [3], and photoluminescence (PL) [4] are techniques that have been used for the nondestructive (n, m) characterization of SWNT species. For the spectroscopic assignment of the two SWNT indices (n, m) , experimental determination of two nanotube properties is necessary: the electronic transition energies E_{ii} ($i = 1, 2, 3, \dots$, giving the number of the electronic transition energy relative to the Fermi level of the unperturbed SWNT) and the nanotube radial breathing mode (RBM) frequency (ω_{RBM}) [2]. Therefore, once one measures a set of these two SWNT properties, a structural assignment can be made by using a model for the $(E_{ii}, \omega_{\text{RBM}})$ to (n, m) transformation. In this Letter we present extensive Stokes and anti-Stokes RRS measurements, leading to a high accuracy characterization of $(E_{ii}, \omega_{\text{RBM}})$ pairs for 46 specific (n, m) SWNTs based on the observation of geometrical patterns in a E_{ii} vs ω_{RBM} plot. We here discuss the dependence of E_{ii} and ω_{RBM} on nanotube structure, and on environmental and thermal effects.

Figure 1 presents Stokes resonance Raman measurements of carbon nanotubes grown by high pressure gas-phase decomposition of CO (HiPco) process, dispersed in aqueous solution, and wrapped with sodium dodecyl sul-

fate (SDS) [5], in the frequency region of the RBM features. We use a Dilor XY triple-monochromator spectrometer and a tunable laser system which allows an almost continuous change of the excitation laser energies (E_{laser}) in the range between 1.52 and 2.71 eV with 76 values of E_{laser} available. This quasicontinuous variation of E_{laser} provides us with detailed information about the evolution of the RBM Raman spectra as a function of

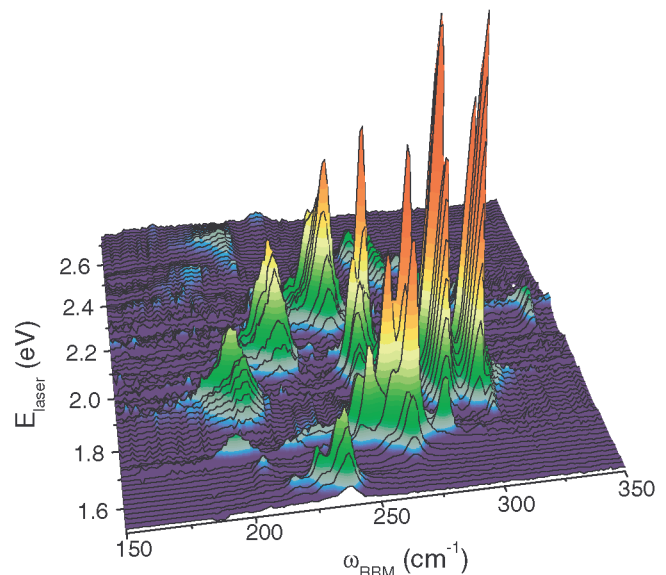


FIG. 1 (color online). RBM Raman measurements of HiPco SWNTs dispersed in SDS aqueous solution [5], measured with 76 different laser lines E_{laser} . The nonresonance Raman spectrum from a separated CCl_4 solution is acquired after each RBM measurement, and is used to calibrate the spectral intensities and to check the frequency calibration.

E_{laser} . Several RBM peaks appear in Fig. 1, each peak corresponding to a carbon nanotube in resonance with E_{laser} , thereby delineating for each nanotube the resonance window (Raman intensity as a function of the energy in the range where the RBM feature can be observed). The same procedure is performed for HiPco SWNTs in bundles (as grown, not dispersed in solution), and both Stokes and anti-Stokes spectra are taken.

This experiment can be used to determine, from RRS measurements, the two sets of information (E_{ii} , ω_{RBM}) for each (n , m) nanotube. The frequency determination ω_{RBM} is directly given in the Raman spectra with 1.0 cm^{-1} accuracy. The electronic transition energy determination E_{ii} is obtained by analyzing the resonance window for each RBM peak, as discussed below.

From these measurements, plots of the Stokes and anti-Stokes Raman peak intensities for each RBM frequency versus E_{laser} (i.e., the experimental resonance windows) are determined. For example, Fig. 2 shows the resulting resonance windows for the same (n , m) SWNT, in different environments, i.e., dispersed in aqueous solution (left) and within a solid bundle (right). Stokes and anti-Stokes resonance windows are shifted from each other in energy due to the difference in the emission energies, given by the $\pm E_{\text{ph}}$ term in the equation for the E_{laser} dependent resonance Raman intensity [6,7]:

$$I(E_{\text{laser}}) \propto \left| \frac{1}{(E_{\text{laser}} - E_{ii} - i\Gamma)(E_{\text{laser}} \pm E_{\text{ph}} - E_{ii} - i\Gamma)} \right|^2, \quad (1)$$

where the matrix elements for optical absorption, electron-phonon interaction, and optical emission are considered here to be constant. E_{ph} is the phonon energy and Γ gives the broadening (FWHM) of the resonance window. Here, we have considered a delta function $\delta(E -$

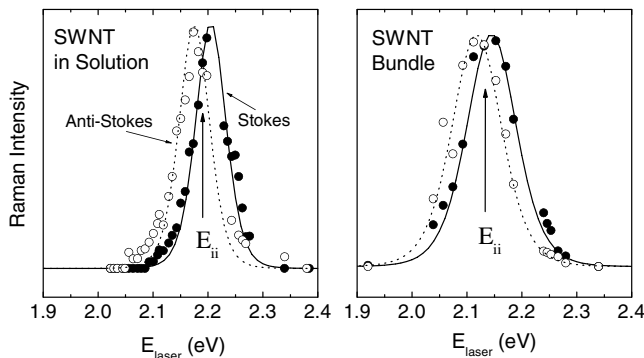


FIG. 2. Stokes (solid symbols) and anti-Stokes (open symbols) experimental resonance windows obtained for the same (n , m) nanotube ($\omega_{\text{RBM}} = 244.4 \text{ cm}^{-1}$) dispersed in aqueous solution and wrapped with SDS (left) and in a bundle (right). The curves show fits to Stokes (solid lines) and anti-Stokes (dotted lines) processes using Eq. (1). The left (right) graph was fit using $E_{ii} = 2.19$ (2.13) eV and $\Gamma = 65$ (112) meV.

E_{ii}) to describe each van Hove singularity in the density of electronic states for a SWNT [1].

The intersection points between the Stokes and anti-Stokes resonance windows [see arrows in Fig. 2] give the transition energies E_{ii} accurately (to $\pm 10 \text{ meV}$). The intensity for the anti-Stokes resonant windows are normalized by the relation $I_{\text{AS}}/I_{\text{S}} = n(E_{\text{ph}})/[n(E_{\text{ph}}) + 1]$ where $n(E_{\text{ph}}) = 1/[\exp(E_{\text{ph}}/k_B T) - 1]$ is the Bose-Einstein thermal factor. For the SWNTs in solution, $T = 300 \text{ K}$ in the Boltzmann factor normalizes the Stokes and anti-Stokes resonance windows, so that there is no heating due to laser power. By comparing the resonance windows for HiPco nanotubes in solution and within solid bundles (as grown), we observed that the resonance window for the bundled SWNTs is broadened and down-shifted in energy in comparison with SWNTs in solution. We have found $\Gamma = 60 \text{ meV}$ on average for SDS wrapped SWNTs in solution and $\Gamma = 120 \text{ meV}$ for SWNTs in bundles, while the room temperature value reported for an isolated SWNT on a Si/SiO₂ substrate is $\Gamma = 8 \text{ meV}$ [8]. Another important observation is a thermal effect due to laser heating observed for the bundled sample. Stokes versus anti-Stokes resonance window measurements using low laser power ($\sim 0.5 \text{ mW}$ focused on a $2 \mu\text{m}^2$ spot in the sample) show that the local temperature is $T \sim 400 \text{ K}$.

Figure 3(a) shows the diameter dependence of the E_{ii} calculated using a nearest-neighbor tight binding (TB) model [1]. Solid circles and squares represent, respectively, semiconducting and metallic nanotubes. The geometrical patterns for carbon nanotube families with $(2n + m) = \text{const}$ (solid gray lines) for E_{22}^S , E_{11}^M , and E_{33}^S are also shown, and the numbers in Fig. 3(a) correspond to the values of $(2n + m)$. For semiconducting nanotubes, it is possible to see separately in Fig. 3(a) the two classes: S1 [$(2n + m) \bmod 3 = 1$] and S2 [$(2n + m) \bmod 3 = 2$], deviating in opposite directions from the $E_{ii} \propto 1/d_i$ line due to their opposite dependence on the chiral angle. Figure 3(b) plots the experimental results obtained for E_{ii} vs ω_{RBM} for each SWNT observed in Fig. 1. The (E_{ii} , ω_{RBM}) results [Fig. 3(b)] can be compared with TB predictions [Fig. 3(a)], and the different E_{ii} electronic transitions for semiconducting (E_{22}^S and E_{33}^S) and metallic (E_{11}^M) tubes, solid circles, and squares, respectively, are clearly seen. Although the energies do not match due to the simplicity of the TB method, the geometrical patterns observed can be compared with the patterns predicted, and the comparison leads to the (n , m) assignment. From the (n , m) assignment for E_{22}^S , we obtain the relation $\omega_{\text{RBM}}(\text{cm}^{-1}) = 223/d_t(\text{nm}) + 10$ for semiconducting SWNTs in an aqueous solution wrapped with SDS. The deviation of the experimental points from this relation is smaller than $\pm 1\%$ of ω_{RBM} . From this relation and comparing the geometrical patterns, we obtain the assignment to E_{33}^S .

The open circles in Fig. 3(b) represent the previously reported values for E_{22}^S transitions in SDS wrapped nano-

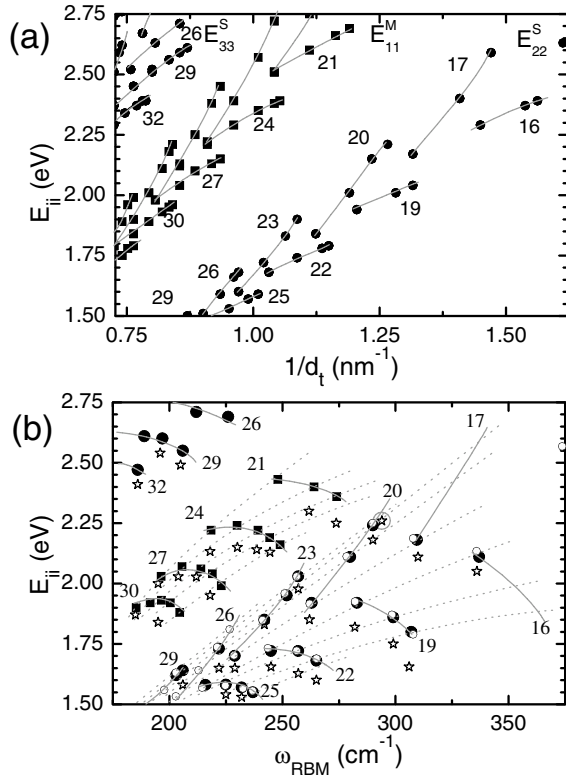


FIG. 3. (a) E_{ii} vs $1/d_t$ plot for SWNTs based on the tight binding model with $\gamma_0 = 2.9$ eV and $s = 0$ [1]. (b) Experimental plot E_{ii} vs ω_{RBM} similar to (a) for 46 different (n, m) carbon nanotubes measured by resonance Raman spectroscopy. Solid circles and solid squares, respectively, denote semiconducting and metallic SWNTs wrapped with SDS in aqueous solution. Open stars are for SWNTs in bundles. Open circles are the photoluminescence results for SWNTs wrapped in SDS [9] scaled by $\omega_{\text{RBM}} = 223/d_t + 10$. Solid and dotted lines, respectively, delineate nanotubes belonging to families of constant $(2n + m)$ and constant $(n - m)$. The $2n + m$ value for each $(2n + m) = \text{const}$ family is indicated in both figures.

tubes in aqueous solution obtained by PL experiments [4,9]. Using the relation ω_{RBM} vs d_t obtained by our (n, m) assignments, the results show good agreement overall between the E_{ii} values obtained from RRS and PL data (taken on similar samples). The largest deviation between E_{ii} obtained by Raman and PL is 35 meV for the (6, 4) SWNT.

The electronic transition energies for metallic SWNTs, not observed in the PL studies, are also determined by RRS (solid squares in Fig. 3(b)). The formation of families of constant $(2n + m)$ is also observed. Surprisingly, the expected splitting in the E_{11}^M van Hove singularities caused by the trigonal warping effect [1,10] is not observed optically for the RBM feature [see Fig. 3(b)]. We only observe the lower energy component of E_{11}^M for each (n, m) SWNT.

The families observed in the geometrical pattern for the metallic nanotube data are also used to find their

(n, m) assignments. We obtain the relation $\omega_{\text{RBM}} = 218/d_t + 17$ for metallic nanotubes, in agreement with previous work within the resolution of the spectrometer [11], leading to an equivalent assignment. Table I shows the experimental values for ω_{RBM} , E_{11}^M , E_{22}^S , E_{33}^S , and the (n, m) assignments thus obtained for both semiconducting and metallic SDS wrapped nanotubes in solution.

The $(E_{ii}, \omega_{\text{RBM}})$ results obtained for bulk HiPco nanotubes in bundles are also presented in Fig. 3(b) by stars. Interestingly, we observe, for HiPco SWNTs in bundles, the zigzag SWNT (10, 0) [circled star in Fig. 3(b)] that had not been previously observed, either by PL studies [4] or by RRS on SDS wrapped SWNTs. The present observation of the missing $(n, 0)$ SWNT gives support to the (n, m) assignment presented here, which is equivalent to the (n, m) assignment previously proposed by Bachilo *et al.* [4], since the four expected SWNTs are here all observed for the $(2n + m) = 20$ family.

TABLE I. Experimental E_{ii} (eV) and ω_{RBM} (cm^{-1}) obtained by RRS for semiconducting and metallic HiPco SWNTs in SDS aqueous solution. The accuracy is ± 10 meV for E_{ii} and ± 1 cm^{-1} for ω_{RBM} .

(n, m)	ω_{RBM}	E_{22}^S	E_{33}^S	(n, m)	ω_{RBM}	E_{11}^M
(6, 4)	337.5	2.11		(7, 7)	248.0	2.43
(6, 5)	309.6	2.18		(8, 5)	264.0	2.43
(7, 5)	282.3	1.92		(8, 8)	218.5	2.22
(7, 6)	263.0	1.92		(9, 3)	274.0	2.35
(8, 3)	297.9	1.86		(9, 6)	230.0	2.24
(8, 4)	280.0	2.11		(9, 9)	196.4	2.03
(8, 6)	245.0	1.72		(10, 4)	239.2	2.22
(8, 7)	230.0	1.70		(10, 7)	205.6	2.07
(9, 1)	307.0	1.8		(11, 2)	244.4	2.19
(9, 2)	290.0	2.24		(11, 5)	214.0	2.06
(9, 4)	257.0	2.03		(11, 8)	185.4	1.90
(9, 5)	242.0	1.85		(12, 0)	247.0	2.16
(9, 7)	216.4	1.58		(12, 3)	219.0	2.04
(10, 0) ^a	294.0 ^a	2.26 ^a		(12, 6)	191.6	1.92
(10, 2)	265.0	1.68		(13, 1)	223.0	2.02
(10, 3)	252.7	1.95		(13, 4)	196.5	1.93
(10, 5)	225.4	1.58		(14, 2)	200.5	1.92
(10, 6)	212.0		2.71			
(11, 1)	257.8	1.72		(15, 0)	204.6	1.88
(11, 3)	231.9	1.57				
(11, 4)	222.0	1.73				
(11, 7)	189.0		2.61			
(12, 1)	236.9	1.55				
(12, 2)	226.0		2.69			
(12, 5)	197.0		2.60			
(13, 3)	203.0	1.62				
(14, 1)	206.0	1.64	2.55			
(15, 2) ^b	186.0		2.47			

^aValues obtained for (10, 0) SWNT within bundles.

^bThis SWNT can be alternatively assigned as (14, 4).

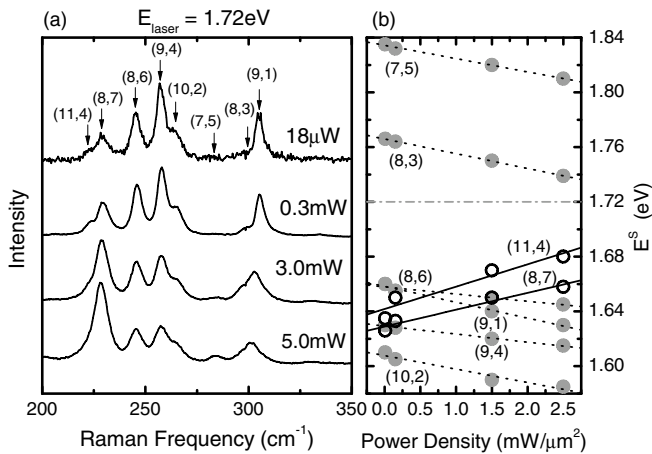


FIG. 4. (a) Dependence of the RBM spectra for HiPco SWNTs in bundles on the laser excitation power for a fixed $E_{\text{laser}} = 1.72$ eV. (b) Dependence of the transition energies on the laser power density. Gray dots and open circles are for S1 and S2 nanotubes, respectively.

The ω_{RBM} value is observed to be the same for semiconducting SWNTs in solution and in bundles within experimental precision. However, an average 70 meV redshift in E_{ii} is observed experimentally for the bundled SWNTs relative to the E_{ii} found for SDS wrapped isolated SWNTs in aqueous solution, although the redshifts are different (from 20 up to 140 meV) for different (n, m) SWNTs. The different redshifts are mainly related to a strong (n, m) -dependent thermal effect due to laser heating that causes changes in the E_{ii} values obtained for the HiPco bundle sample.

To characterize the (n, m) -dependent laser heating effect on the Raman spectra for the SWNT bundle sample, measurements have been performed by changing the laser intensity on the HiPco SWNT bundle sample for eight different laser energies. The dependence of the RBM spectra on the laser intensity for a fixed $E_{\text{laser}} = 1.72$ eV is shown in Fig. 4(a), indicating that the relative intensities of the RBM peaks change by increasing the laser power, showing that the electronic structure is dependent on the sample heating. The changes in spectra are reversible, showing that no damage or decomposition occurs in this heating process. We have determined the transition energies for each (n, m) nanotube as a function of the laser power density using the resonance window obtained experimentally for each RBM peak. The results for the transition energies as a function of the laser power density for each of the eight SWNTs assigned in Fig. 4(a) are presented in Fig. 4(b). The transition energies move in opposite directions when the laser power increases for semiconducting nanotubes of the S1 type (dotted lines) and of the S2 type (solid lines); they undergo a downshift for S1 semiconducting nanotubes and an up-shift for S2 nanotubes (similar to the uniaxial strain-enhanced effect on SWNT bundles recently reported [12]), thus explaining the changes in the relative intensities for the

RBM peaks observed with a single E_{laser} [Fig. 4(a)]. The variation in the E_{ii} value [line slopes in Fig. 4(b)] caused by an increase in the laser power, is larger for SWNTs with smaller chiral angles. The lines associated with S1 nanotubes with larger and smaller slopes are indicated in Fig. 4(b) and represent, respectively, nanotubes (9, 1) and (8, 6), which have the smallest ($\theta = 5.2^\circ$) and largest ($\theta = 25.3^\circ$) chiral angles in Fig. 4.

In summary, we obtain $(E_{ii}, \omega_{\text{RBM}})$ for 46 different (n, m) SWNTs, including 28 semiconducting and 18 metallic SWNTs. The (n, m) assignment based on the experimentally obtained $(E_{ii}, \omega_{\text{RBM}})$ geometrical patterns, and the RRS-derived results are in agreement with previously proposed (n, m) assignments for semiconducting SWNTs, based on PL measurements. Only one low energy component of the E_{11}^M singularity for each metallic SWNT is observed for the RBM spectra and the explanation for this result is an open issue. For the same (n, m) nanotube, the resonance window is redshifted and broadened for SWNTs in bundles as compared to SDS wrapped nanotubes in solution. By increasing the laser power, the E_{22}^S energies of SWNTs in bundles are redshifted for S1 [$(2n + m) \bmod 3 = 1$] nanotubes and blueshifted for S2 [$(2n + m) \bmod 3 = 2$] nanotubes, relative to the average 70 meV redshift, showing that the trigonal distortion of the electronic structure increases with temperature. The connection between the present results and the results for double-wall carbon nanotubes [13] and SWNTs on SiO_2 substrates [2] is still an open issue.

The authors acknowledge Dr. R. Capaz, Professor R. Saito, and Dr. J. Maultzsch for helpful discussions and A. J. Mai, Jr., for help with the experimental work. This work was supported by the Brazilian agencies FAPEMIG, CNPq, CAPES, and by Instituto do Milênio de Nanociências, MCT, Brazil. M. S. D acknowledges support under NSF DMR 01-16042.

- [1] R. Saito, G. Dresselhaus, and M. S. Dresselhaus, *Physical Properties of Carbon Nanotubes* (Imperial College Press, London, 1998).
- [2] A. Jorio *et al.*, Phys. Rev. Lett. **86**, 1118 (2001).
- [3] A. Hagen and T. Hertel, Nano Lett. **3**, 383 (2003).
- [4] S. M. Bachilo *et al.*, Science **298**, 2361 (2002).
- [5] M. J. O'Connell *et al.*, Science **297**, 593 (2002).
- [6] R. M. Martin and L. M. Falicov, *Light Scattering in Solids*, Topics in Applied Physics Vol. 8 (Springer-Verlag, Berlin, 1975), pp. 79–145.
- [7] M. A. Pimenta *et al.*, Phys. Rev. B **58**, R16 016 (1998).
- [8] A. Jorio *et al.*, Phys. Rev. B **63**, 245416 (2001).
- [9] R. B. Weisman and S. M. Bachilo, Nano Lett. **3**, 1235 (2003).
- [10] P. Kim *et al.*, Phys. Rev. Lett. **82**, 1225 (1999).
- [11] M. S. Strano *et al.*, Nano Lett. **3**, 1091 (2003).
- [12] M. Lucas and R. J. Young, Phys. Rev. B **69**, 085405 (2004).
- [13] M. Hulman *et al.*, New J. Phys. **6**, 1 (2004).